

Journal of Biomedical Optics

BiomedicalOptics.SPIEDigitalLibrary.org

Extraction of optical properties and prediction of light distribution in rat brain tissue

Mehdi Azimipour
Ryan Baumgartner
Yuming Liu
Steven L. Jacques
Kevin Eliceiri
Ramin Pashaie

Extraction of optical properties and prediction of light distribution in rat brain tissue

Mehdi Azimipour,^a Ryan Baumgartner,^a Yuming Liu,^b Steven L. Jacques,^{c,d} Kevin Eliceiri,^b and Ramin Pashaie^{a,*}

^aUniversity of Wisconsin-Milwaukee, Electrical and Computer Engineering Department, Milwaukee, Wisconsin 53211

^bUniversity of Wisconsin at Madison, Laboratory for Optical and Computational Instrumentation, 1675 Observatory Drive, Madison, Wisconsin 53706

^cOregon Health Science University, Department of Biomedical Engineering, 3303 SW Bond Avenue, Portland, Oregon 97239

^dOregon Health Science University, Department of Dermatology, 3303 SW Bond Avenue, Portland, Oregon 97239

Abstract. Predicting the distribution of light inside any turbid media, such as biological tissue, requires detailed information about the optical properties of the medium, including the absorption and scattering coefficients and the anisotropy factor. Particularly, in biophotonic applications where photons directly interact with the tissue, this information translates to system design optimization, precision in light delivery, and minimization of unintended consequences, such as phototoxicity or photobleaching. In recent years, optogenetics has opened up a new area in deep brain stimulation with light and the method is widely adapted by researchers for the study of the brain circuitries and the dynamics of neurological disorders. A key factor for a successful optogenetic stimulation is delivering an adequate amount of light to the targeted brain objects. The adequate amount of light needed to stimulate each brain object is identified by the tissue optical properties as well as the type of opsin expressed in the tissue, wavelength of the light, and the physical dimensions of the targeted area. Therefore, to implement a precise light delivery system for optogenetics, detailed information about the optical properties of the brain tissue and a mathematical model that incorporates all determining factors is needed to find a good estimation of light distribution in the brain. In general, three measurements are required to obtain the optical properties of any tissue, namely diffuse transmitted light, diffuse reflected light, and transmitted ballistic beam. In this report, these parameters were measured *in vitro* using intact rat brain slices of 500 μm thickness via a two-integrating spheres optical setup. Then, an inverse adding doubling method was used to extract the optical properties of the tissue from the collected data. These experiments were repeated to cover the whole brain tissue with high spatial resolution for the three different cuts (transverse, sagittal, and coronal) and three different wavelengths (405, 532, and 635 nm) in the visible range of the spectrum. A three-dimensional atlas of the rat brain optical properties was constructed based on the experimental measurements. This database was linked to a Monte Carlo toolbox to simulate light distribution in the tissue for different light source configurations. © 2014 Society of Photo-Optical Instrumentation Engineers (SPIE) [DOI: 10.1117/1.JBO.19.7.075001]

Keywords: optogenetics; absorption coefficient; scattering coefficient; anisotropy factor; integrating sphere; inverse adding doubling; Monte Carlo simulation.

Paper 140237R received Apr. 14, 2014; revised manuscript received Jun. 4, 2014; accepted for publication Jun. 5, 2014; published online Jul. 4, 2014.

1 Introduction

There has been tremendous interest in recent years in implementing new techniques for optical stimulation of neurons. Optical stimulation is often considered the superior technology, compared with electric stimulation, since the inherent parallelism of optics allows researchers to excite or inhibit the activity of cells in large-scale networks of the brain. Among all developed techniques, optogenetics has become the most popular and widely used method for the study of the dynamics of the brain and circuitry of neurological and psychiatric disorders. In optogenetic brain stimulation, specific cell-types of interest, on the surface or inside the brain tissue, are genetically targeted to express certain light-gated ion channels or ion pumps.^{1–8} Once these proteins are produced in a cell, the activity of the cell can be increased or suppressed simply by exposing the cell to specific wavelengths, mostly in the visible range of the spectrum. Obviously, delivering an adequate amount of light

to stimulate the target area within the brain is an important step in the design of all optogenetic experiments. An insufficient amount of light cannot generate effective stimulation, whereas excessive light intensity can potentially cause damage to the tissue or penetrate deeper and stimulate other brain objects. In optogenetic stimulation, the amplitude of the induced photocurrent in a neuron depends on multiple factors, including biological variables such as the kinetics of the expressed opsin⁹ and optical properties of the tissue, as well as system design variables such as the intensity and wavelength of light. Two separate approaches have been explored for light delivery in optogenetics. For cortical stimulation and superficial areas, spatial light modulators, such as MEMS devices¹⁰ or liquid crystals,^{11,12} are employed to generate complex and even three-dimensional (3-D) patterns of light distributions inside tissue. However, to target deep brain objects, optical fibers are implanted to guide and deliver laser pulses to the region of interest.^{3,4,13–15}

*Address all correspondence to: Ramin Pashaie, E-mail: pashaie@uwm.edu

Predicting the light intensity delivered by an optical fiber to a target area in the brain is necessary for proper *in vivo* optogenetic stimulation and has been briefly studied before. A simplified Kubelka-Munk model,¹⁶ which neglects the absorption coefficient, was proposed by Aravanis et al.¹⁵ and later by Stark et al.¹⁷ To develop this model, they conducted a sequence of experiments and measured the intensity of the transmitted light through mouse brain slices of different thicknesses, then used this experimental data to formulate a set of equations which estimate the axial variations of light intensity inside the brain tissue. More recently, Al-Juboori et al.¹⁸ used the fiber punch-through method to measure the effective attenuation coefficient of different areas of the mouse brain and employed the Beer-Lambert law to measure the effective attenuation coefficient in tissue slices of 600 μm thickness. Then, based on the extracted optical properties, the diffusion equation in one-dimension was adapted to determine the required input light intensity needed to deliver the desired optical power to target a deep brain object. Although this approach offers a systematic pathway to measure the tissue effective attenuation coefficient, it is still unable to clarify other optical properties that are essential for precise estimation of light distribution in any turbid medium. Moreover, these models do not incorporate the impact of the tissue heterogeneity on light distribution in the medium.

Obviously, an initial requirement for the design of all biophotonic experiments (including optogenetic stimulation) or related therapeutic protocols is obtaining reasonable estimates of the optical properties of tissue.¹⁹ In most published literature, tissue optical properties are parameterized by three variables: the absorption coefficient, μ_a , the scattering coefficient, μ_s , and the anisotropy factor, g .¹⁶ The mathematical models that are developed to emulate light transport in turbid media use these variables to estimate the distribution and penetration depth of light within the medium.¹⁹ These phenomenological properties of biological tissue can be measured *in vivo* or *in vitro*. For *in vivo* measurements, multiple time-domain or frequency-domain methods have been developed with instrumentation such as confocal microscopy and optical coherence tomography used to collect the raw data.²⁰ Then, the values of tissue optical properties are extracted from the raw data by solving a set of inverse problems.^{21–23} Data acquisition *in vitro* is performed mostly by using double-integrating-sphere setups,²⁴ which are used to measure the total diffuse reflection and transmission and the intensity of the transmitted ballistic beam. By making these three measurements and using mathematical algorithms, e.g., inverse adding doubling (IAD) method,²⁵ the optical properties of the tissue under test are estimated.

In this paper, we present an approach to measure the three variables that define optical properties for the rat brain tissue. To extract the values of these parameters, 500- μm brain slices were prepared and scanned by two customized optical setups and the diffuse transmittance, diffuse reflectance, and ballistic transmittance for each slice were measured with high spatial sampling rate of 3000 points per square centimeter. These measurements were made for three different cuts (transverse, sagittal, and coronal) and three different wavelengths, 405, 532, and 635 nm, to cover the visible range of the spectrum. Then, the IAD method²⁵ was employed to reconstruct the optical properties of the tissue using the collected experimental data. By repeating this procedure for all slices, a 3-D database of the tissue optical properties was developed. Next, this database was

connected to our 3-D Monte Carlo toolbox^{26,27} to simulate light-tissue interactions and find a reasonable estimation of the distribution of light inside the tissue. The developed software incorporates the effect of tissue heterogeneities, physical parameters of the source, including optical fiber core diameter, numerical aperture (NA), or beam type, such as uniform or Gaussian,²⁸ and the wavelength of the source to offer a more accurate model for light distribution in the brain. The process of extracting tissue optical properties is shown in Fig. 1.

2 Material and Methods

2.1 Sample Preparation

In these experiments, 27 female Sprague-Dawley rats weighing from 250 to 300 g were used. All animal procedures were approved by the University of Wisconsin-Milwaukee Institutional Animal Care and Use Committee and were conducted in accordance with National Institute of Health standards on the humane treatment of laboratory animals. Animals were anesthetized by isoflurane (1.5 to 2% oxygen) before decapitation by a lab guillotine. The intact brain tissue was extracted from each animal and fixed on an agarose block for slicing. Next, transverse, sagittal, and dorsal brain slices of 500 μm thicknesses were cut using a vibratome (Lancer vibratome series 1000, St. Louis, Missouri) while the brain was submerged in phosphate buffered saline solution (Sigma-Aldrich, St. Louis, Missouri) and cooled by dry ice. Then, fresh slices were loaded into the optical setup displayed in Fig. 2 and scanned one slice at a time. In each round, one slice was cut and scanned during the period the vibratome was cutting the next slice. To minimize the timing of the experiment during which the brain is kept in the freezing solution to preserve the tissue and its optical properties, it is important to synchronize the slicing and the scanning procedures. In our experience, following this protocol, the optical properties did not have significant change during the scanning of each slice and it took ~ 2 h to complete the whole brain scan.

2.2 Measurement Procedures

2.2.1 Measuring diffuse reflectance and transmittance

Based on the IAD model, three different measurements (diffuse reflectance, diffuse transmittance, and ballistic transmittance)

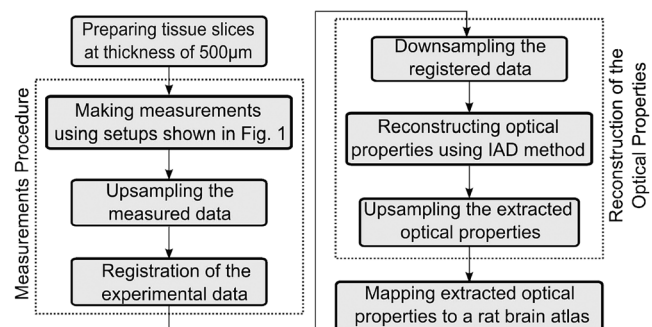


Fig. 1 The algorithm adapted for extracting tissue optical properties. The process starts with sample preparation in which brain slices of 500 μm thickness are produced and scanned by the customized optical setups shown in Fig. 2. Next, the inverse adding doubling (IAD) reconstruction algorithm is applied to the collected data to extract the value of parameter, which determine the optical properties of the tissue.

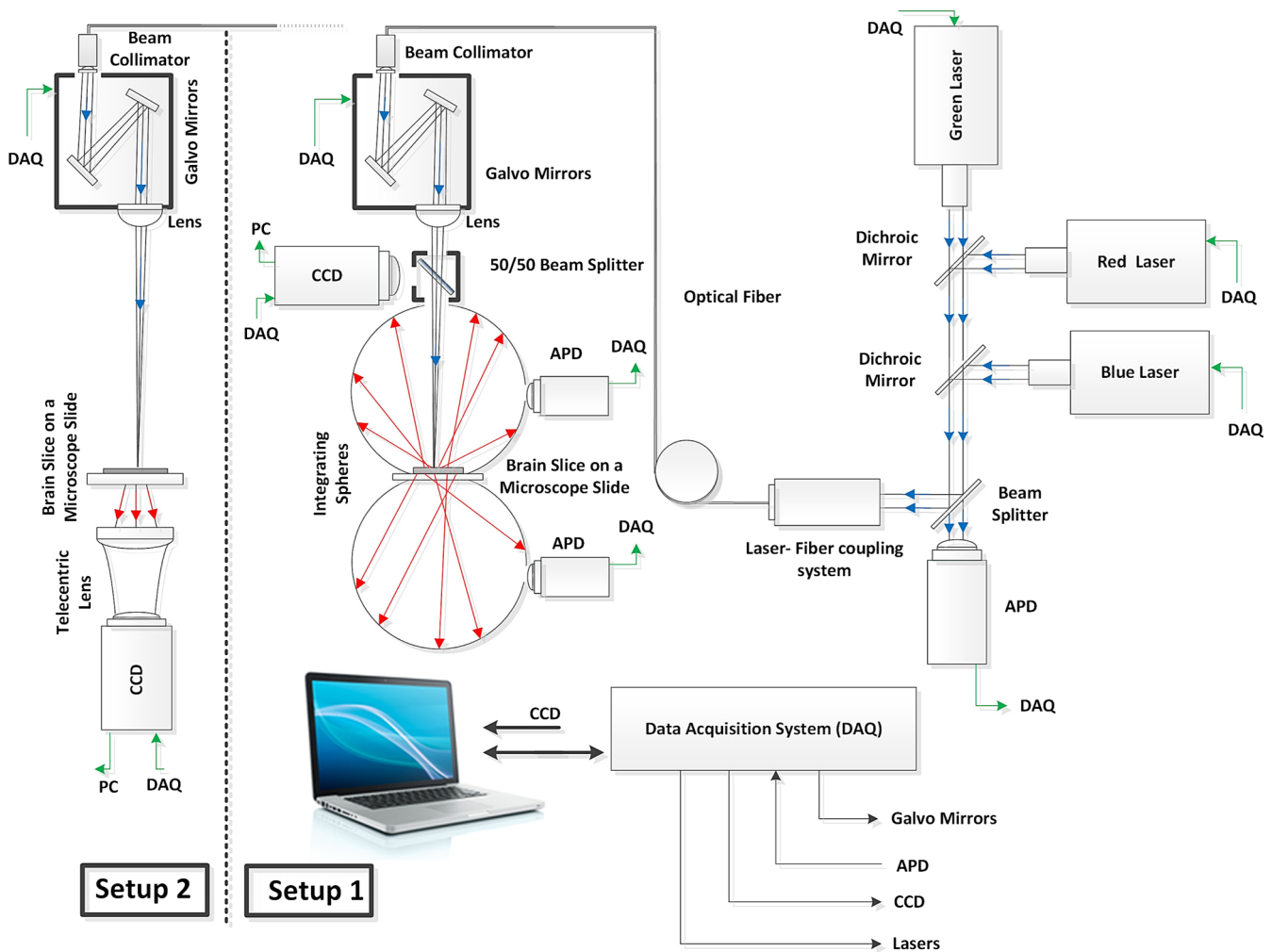


Fig. 2 Schematic of the experimental setups used to measure diffuse reflected and transmitted light (setup 1) and transmitted ballistic light (setup 2).

are required to extract the complete set of tissue optical properties, including μ_a , μ_s , and g .²⁵ Diffuse reflectance and diffuse transmittance were measured simultaneously using optical setup 1 and the ballistic transmittance measurements were performed by optical setup 2, which are both illustrated in Fig. 2. Diffuse reflectance and diffuse transmittance measurements were acquired using the double-integrating-sphere technique. For this experiment, after preparing a brain slice, the slice was placed between two integrating spheres (one two-port, 6-in. CVI Melles Griot BPS integrating sphere with 1.5-in. sample port diameter, and one four-port, 6-in. Spectrafect Integrating Sphere, Newport Corporation, Irvine, California, with 1-in. sample port diameter) and was scanned using a focused laser beam (with three different wavelengths: blue laser Thorlabs 405-nm laser diode, green laser Ultralaser 532-nm diode-pumped solid-state, and red laser Thorlabs 635-nm laser diode) with a 200- μm spot size at the focal point on the sample. The diffuse reflected light intensity, $R(r_s^{\text{direct}}, r_s)$, was measured using a photodetector (Thorlabs, Newton, New Jersey, PDA36A, Si switchable gain detector) that is mounted on the top sphere, and diffuse transmitted light intensity, $T(r_s^{\text{direct}}, r_s)$, was measured by a second photodetector (Thorlabs, APD110A2/M, avalanche photodetector) that was installed on the bottom sphere. The variables reflectance (M_R) and transmittance (M_T), defined by the amount of light reflected by and transmitted through the

sample normalized to the intensity of the incoming light, respectively, were calculated using the following set of equations:²⁵

$$M_R \equiv r_{\text{std}} \cdot \frac{R(r_s^{\text{direct}}, r_s) - R(0, 0)}{R(r_{\text{std}}, r_{\text{std}}) - R(0, 0)}$$

$$M_T \equiv \frac{T(r_s^{\text{direct}}, r_s) - T_{\text{dark}}}{T(0, 0) - T_{\text{dark}}}. \quad (1)$$

In these equations, parameters $R(0, 0)$, $T(0, 0)$, and T_{dark} are calibration measurements, and r_{std} is the wall reflectance coefficient of the integrating sphere. More details of the calibration and measurement process are available in Ref. 25.

By using a galvo scanner (Te-Lighting, China, PT-30K laser scanner galvo system kits) for each brain slice, M_R and M_T variables were measured with a spatial resolution of 3000 points per square centimeter as discussed later. In our measurements, we utilized a CCD camera to obtain the geometry of the tissue and used this information to avoid scanning the empty areas around or within the slice to speed up the scanning process. Therefore, it was necessary to register the galvo scanner on the camera output. The registration was carried out by formulating the relationship between the voltages applied to the scanning mirrors of the galvo system and the coordinates of the laser beam on the tissue, which was recorded by the camera. For this purpose, four

different voltages were applied to the scanning mirrors while the camera was monitoring the position of the beam, and the system used this information to map the position of the scanning mirrors on the pixels of the CCD camera. The registration needs to be done only once during the whole experiment. Then, for each slice, the geometrical shape was obtained by capturing a picture of the brain slice by the CCD camera, and this image was used as a mask to separate the tissue from the background. The developed binary mask defines the region of interest (ROI) which includes just the tissue area. This complex ROI also excludes the edges of the tissue where measurements are not accurate and also the footprints of ventricles within each slice. The process of scanning and data acquisition for each slice took ~ 1 min., and it was controlled through a custom software developed using LabVIEW (LabVIEW 8.2, National Instruments Corp., Austin, Texas). The procedure for system calibration and data evaluation are discussed in Appendix A.

2.2.2 Measuring ballistic transmittance

In the ballistic transmittance test, we measured the percentage of the beam that passes through a sample with no scattering or absorption. Traditionally, for this test, a photodetector is used to measure the intensity of the beam that passes directly through the sample in combination with an aperture placed in front of the detector that rejects the scatterer rays. For heterogeneous samples, such as brain slices, this test can be performed either by moving the sample or possibly the aperture and the photodetector, which makes the process quite time consuming. To avoid this problem, we used a telecentric lens system instead of the aperture, which only passes and projects the collimated portion of the transmitted beam onto a CCD rather than the

photodetector.²⁹ In these experiments, each brain slice was placed on a sample holder between the galvo mirrors and the camera and once again the slice was scanned with the same spatial resolution of 3000 points per square centimeter (see Fig. 2). Similar to the previous measurements, only the tissue area was scanned. By processing the captured frame, the intensity of the ballistic beam was computed by integrating the values of all the pixels within a circular area that has the same diameter as the reference beam-waist. Then, the transmitted ballistic beam ratio was calculated using the following equation:

$$M_U = \frac{I_B - I_N}{I_R - I_N}, \quad (2)$$

where I_N is the mean value of the background noise intensity when the laser beam is blocked, I_B is the intensity of the transmitted ballistic beam, I_R is the intensity of the reference beam, and $M_U \in [0, 1]$ is the ballistic transmittance. The calibration process, including measuring the intensity of the reference beam (I_R) and the background noise (I_N), needs to be done only once during the whole experiment. To measure the intensity of the reference beam, a predefined voltage was applied to the laser and an image was captured by the CCD camera without any sample in the path. To prevent saturating the camera, a neutral density filter was positioned in front of the CCD sensor to reduce the laser intensity. As described earlier, the summation of all the pixel values inside the beam-waist was calculated to obtain the reference beam intensity (I_R).

In Fig. 3, a sample transverse cut of rat brain and the corresponding interpolated diffuse reflectance, diffuse transmittance, and ballistic transmittance measurements are shown for the green laser (532 nm) measurements. These data are used later to extract

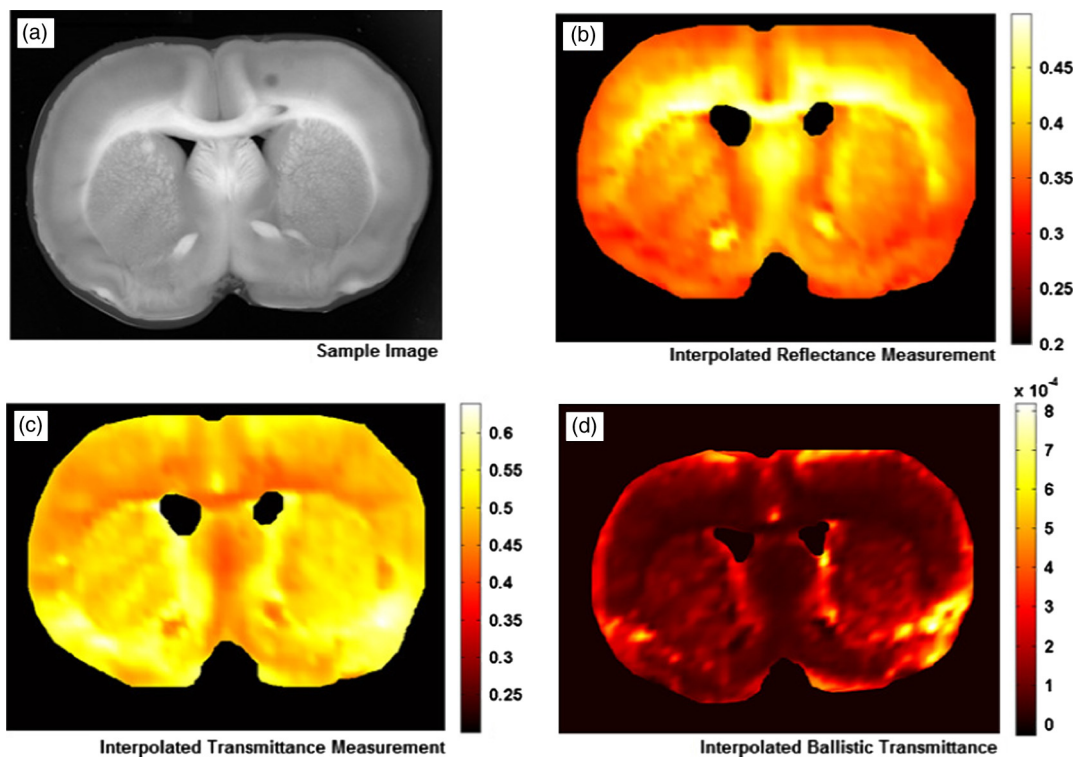


Fig. 3 Results of the scanning process with the green laser wavelength of 532 nm. Data are presented in arbitrary units. (a) Image of a sample brain slice. (b) Interpolated reflectance measurements. (c) Interpolated transmittance measurements. (d) Interpolated ballistic transmittance.

the optical properties of the tissue, including the absorption coefficient, scattering coefficient, and anisotropy factor.

2.2.3 Mapping the experimental data

Since the measurements are made by two different setups, there is a possible displacement between the data collected by these two optical setups. Therefore, before any further process, this displacement should be compensated. We adapted the MATLAB® command “imregister” from the image processing toolbox (MATLAB® 7.14, The MathWorks Inc., Natick, Massachusetts) to register these two datasets. Once the dataset was prepared and displacement was compensated, these data were fed to the IAD code.

3 Extracting Optical Properties

The IAD method is an iterative algorithm designed to extract the optical properties of a homogeneous sample from the measurements discussed in the previous section. The iterations are initiated with some random values assigned to the optical properties of the medium. Then, in each iteration, the algorithm solves the radiative transport equation³⁰ to calculate the transmission and reflection of the sample and compares these results with the experimental data. Next, it readjusts the values of the optical properties to minimize the error between the calculations and experimental results and continues this process until convergence.

As mentioned before, in the IAD method, the assumption is that the sample is a slab with uniform optical properties. To satisfy the homogeneity assumption in IAD algorithm, the scattered light in the tissue should be confined to a small region in which the optical properties remain relatively uniform inside the illuminated area. Our Monte Carlo simulation for light propagation in a slab of turbid medium of thickness $500\ \mu\text{m}$, which has uniform optical properties close to typical values of biological tissue ($\mu_a = 1\ \text{mm}^{-1}$, $\mu_s = 31.6\ \text{mm}^{-1}$, and $g = 0.9$), reveals that the beam width of a laser, which is $200\ \mu\text{m}$ in diameter before the slab, increases to $\sim 500\ \mu\text{m}$ after passing through this scattering medium, as shown in Fig. 4. Therefore, in our experiments, we collected data from discrete sample points and assumed that the optical properties are uniform within the illuminated area for each data point. Then, we used the interpolation to fill the gaps between discrete data points on the tissue.

Once the experimental data are prepared and displacement was compensated, these data were loaded to the IAD code. Since IAD is a time-consuming process, not all of the interpolated data points could be used for reconstruction. In our code, we used only a subset of the sampled data points to extract the optical properties via IAD. In the next step, the density of the extracted optical properties was increased by a two-dimensional bicubic interpolation algorithm.³¹ For

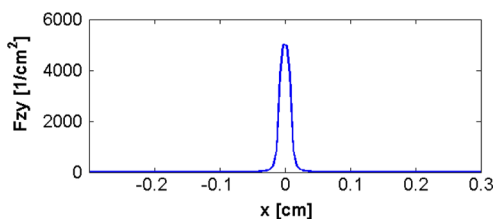


Fig. 4 Lateral distribution of light transmitted through a slab with thickness of $500\ \mu\text{m}$ and typical tissue optical properties when illuminated with a laser beam of $200\ \mu\text{m}$ diameter.

the brain slice shown in Fig. 3(a), reconstructed values of absorption coefficient, reduced scattering coefficient, scattering coefficient, and anisotropy factor are shown in Fig. 5. Another example of such a reconstruction that illustrates the heterogeneity of the brain tissue regarding the optical properties is displayed in Fig. 6.

The described calculation of ballistic transmittance is admittedly approximate, and a more sophisticated deconvolution of the point spread function in angle space of transmitted light versus variable sample thickness would more appropriately define the μ_s and g values. However, when $g \gg 0.5$, the spatial distribution of light is dominated by the lumped parameter $\mu_s^{-1} = \mu_s(1 - g)$, which is reliably specified by the integrating sphere measurements, even in the region of nondiffuse light that occurs near the probe tip. See Appendix B for an illustration of this similarity principle. So the properties of μ_s and g deduced here, even if slightly in error, will still yield reliable predictions of light distribution in the tissue, even near the light source.

4 Results and Discussion

In order to investigate the impact of tissue heterogeneities and different light source configurations on the distribution of light inside tissue, a 3-D Monte Carlo toolbox was prepared and linked to the developed database of the rat brain tissue optical properties. Results of these simulations are presented in the following sections.

4.1 Impact of Brain Tissue Heterogeneity on Light Distribution

For any inhomogeneous medium, such as the brain tissue, we logically expect to observe a different or possibly more complex light distribution pattern compared to the light distribution pattern in a uniform medium of the same volume. To investigate the effect of tissue heterogeneities on light distribution in the brain, we simulated the photon transport process inside the tissue using our 3-D Monte Carlo code and compared our results with the dual homogenous medium. In both simulations, all photons are launched from a uniform source with diameter of $150\ \mu\text{m}$, which is placed at the specified area marked in Fig. 7(a). For the dual homogenous model, the mean value of the optical properties of the whole tissue was assigned as the optical properties of a virtual uniform medium. On the other hand, for the heterogeneous test, we used the extracted database of the optical properties. Optical properties of the tissue in the region are displayed in panels Figs. 7(b) to 7(d). An example of the difference between the light distributions in these two structures is shown in Figs. 7(e) and 7(g), and the corresponding contour maps of the light distributions are displayed in Figs. 7(f) and 7(h). Furthermore, light distribution along an arbitrary axial line is displayed in Fig. 7(i). This result highlights the effect of tissue heterogeneity on light distribution, which, in this experiment, has caused some considerable asymmetry in the distribution pattern in a way that the intensity of light at a distance of $\sim 2.50\ \text{mm}$ on one side is more than three times stronger than the light intensity at the same distance from the center of the source on the other side. The curve in Fig. 7(j) shows the difference between the two distributions that is caused by the heterogeneity in absorption, scattering, and anisotropy factor. Based on our observation, in short distances in the brain tissue, the difference between the light distribution in the homogeneous approximation and the actual heterogeneous model is minimal.

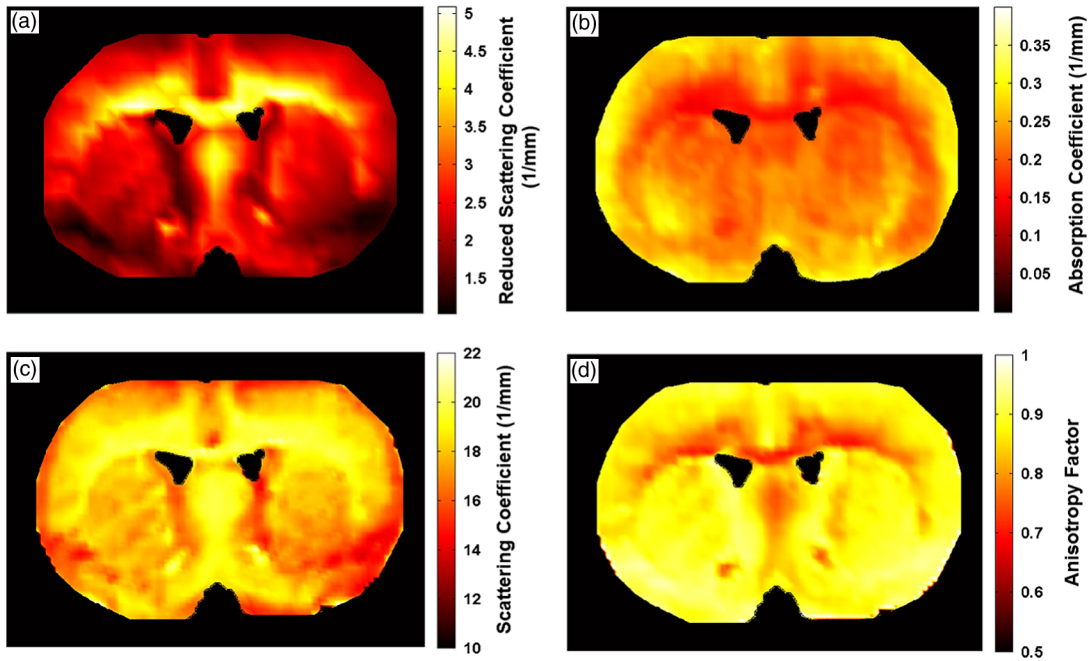


Fig. 5 Extracted optical properties of the rat brain slice produced by IAD algorithm, which is applied to the raw data shown in Fig. 3. (a) Reduced scattering coefficient. (b) Absorption coefficient. (c) Scattering coefficient. (d) Anisotropy factor.

However, as the distance from the source increases, this difference grows. Therefore, the heterogeneity effect in the design of optogenetic experiments is more essential once highly sensitive opsins, such as step-function opsin,⁶ are used. The reason is that in these cases, even low-intensity light that reaches deeper regions of brain tissue can stimulate the cells.

The impact of the tissue heterogeneity on the axial distribution of light is also significant. Figure 8 shows the simulation results in which the axial penetration depth at two different regions, marked by points A and B in the figure, are compared. In this case, at a depth of 2 mm from the fiber tip, light fluence rate for point B is almost five times larger than that for point A.

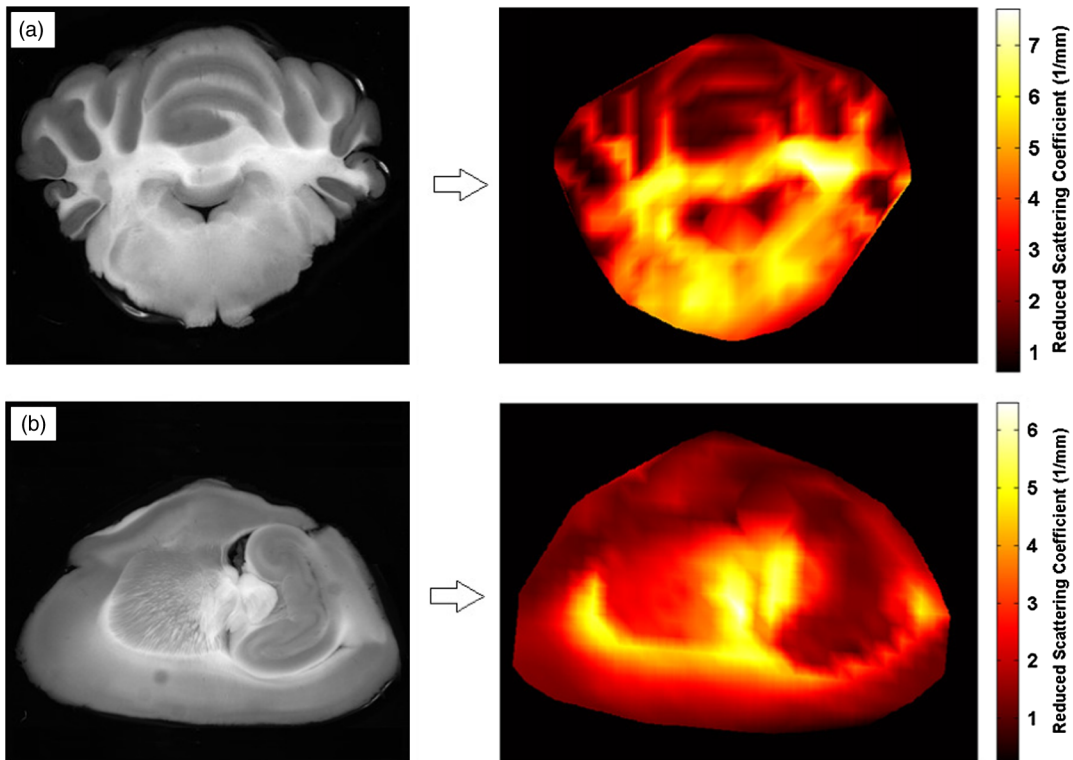


Fig. 6 Extracted reduced scattering coefficient at 532 nm for a rat brain tissue: (a) transverse cut and (b) sagittal cut.

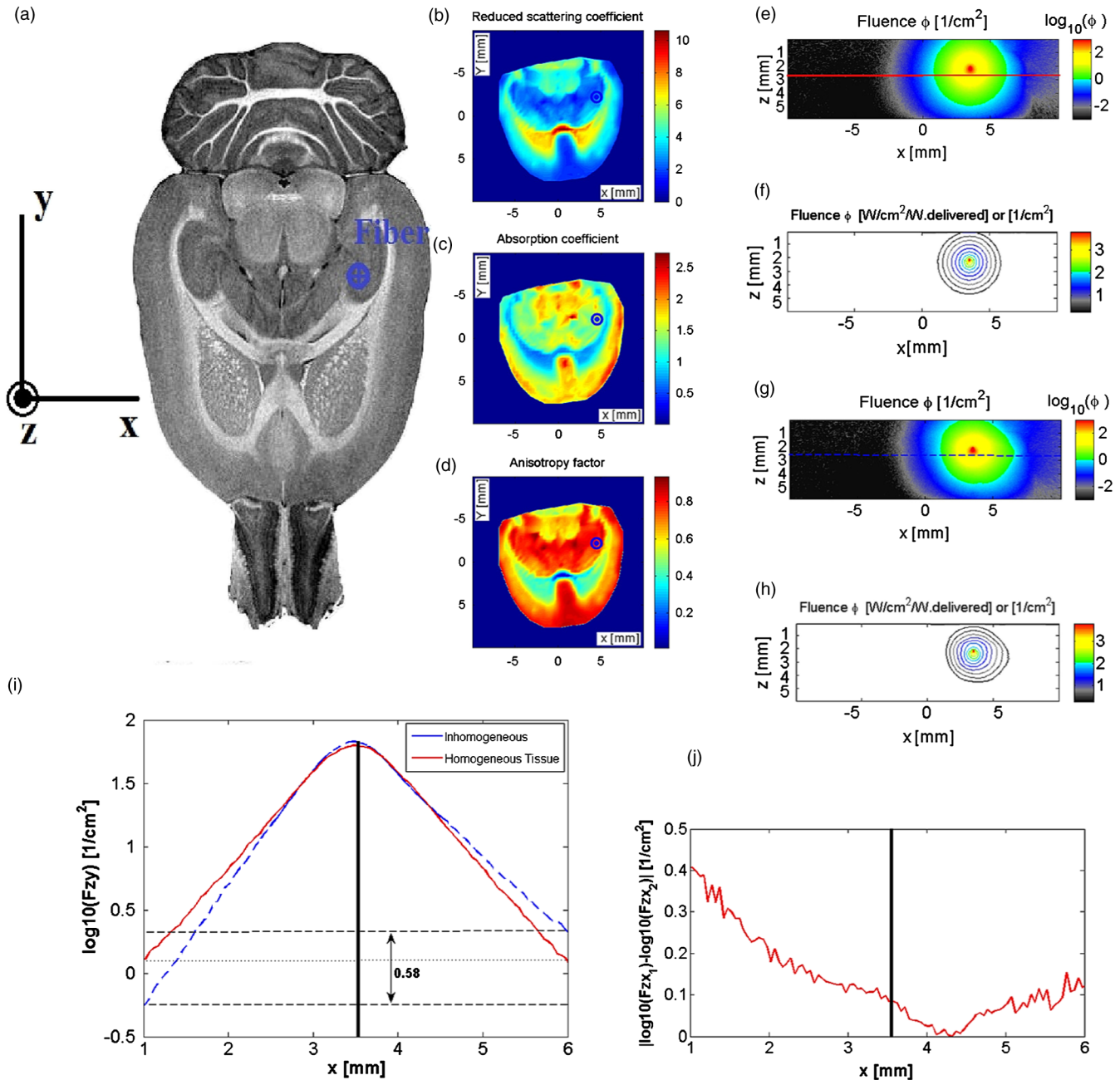


Fig. 7 (a) An optical fiber of 150 μm diameter is placed on the marked area inside the tissue to launch a uniform beam. The three-dimensional Monte Carlo simulations are run by launching 10 million photons. Optical properties of the tissue in the region are displayed in (b) to (d) for a blue laser at 405 nm. (e) Two-dimensional representation of the light distribution in the XZ plane (F_{XZ}) for the homogeneous brain tissue. (f) Contour map of the light distribution in the homogeneous brain tissue. (g) Two-dimensional representation for the distribution of light in the XZ plane (F_{XZ}) for the inhomogeneous brain tissue. (h) Contour maps of the light distribution in the inhomogeneous brain tissue. (i) Lateral fluence rate of the light along the X axis for the inhomogeneous and homogeneous brain tissue, which shows considerable difference between the two distributions. Distribution of the light for homogeneous tissue along the Z axis shows almost an identical change in both directions far from the fiber position (solid curve) while the light distribution has become asymmetric as a result of the tissue heterogeneity (dashed curve). (j) The difference between distribution of light in the homogeneous and inhomogeneous tissue.

4.2 Impact of Physical Parameters of the Source on Light Distribution

Choosing the proper light delivery mechanism is important in optogenetic experiments, particularly when the application demands precise stimulation of some target areas. Optical fibers

are widely used for optogenetic stimulation of deep brain objects *in vivo*.^{3,13–15} Physical parameters of the optical fiber, such as core diameter and NA, have a certain impact on the beam profile and its distribution in the medium. Here, Monte Carlo simulation was used to investigate the light propagation along the tip of

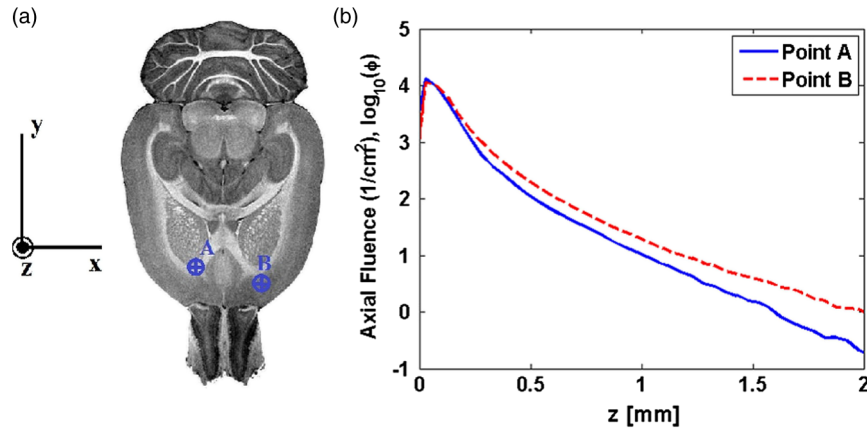


Fig. 8 (a) Optical fiber with $100\ \mu\text{m}$ diameter is placed on the marked regions in the tissue. (b) Comparing the axial fluence rate along z axis for points A and B. The difference between the attenuation coefficients in these two regions has caused significant difference between the axial penetration depth of light at these two positions for a blue laser at 405 nm.

the optical fiber for different fiber parameters and different wavelengths. In Fig. 9(b), the axial fluence rate (light fluence rate along the z direction) for a 405-nm wavelength is shown for different fiber diameters: 200, 150, 100, and $50\ \mu\text{m}$. The simulation results show that for the same optical power, the axial fluence rate decreases when increasing the fiber diameter. On the other hand, it seems that reducing the diameter of the fiber below $100\ \mu\text{m}$ does not have significant impact on the axial fluence rate. Figure 9(c) demonstrates the axial fluence rate for a $100\text{-}\mu\text{m}$ -diameter optical fiber with different NAs, including 0, 0.1, 0.22, and 0.39. According to these results, light intensity drops faster along the axial direction for the optical fibers that have larger NA. Figure 9(d) represents the impact of the wavelength on light distribution. Here, for shorter wavelengths, the attenuation rate is higher as expected.¹⁶ For the blue light (dashed line), the attenuation is higher and the intensity drops much faster than the green and red lights. A comparison

of the axial attenuation between the Gaussian and uniform light source is presented in Fig. 9(e). These data show that the Gaussian beam has a higher fluence rate.

5 Conclusion

In this paper, we present an approach to extract the major optical properties (absorption and scattering coefficients and anisotropy factor) of the rat brain tissue with spatial resolution of ~ 3000 sample points per square centimeter for three different cuts (transverse, sagittal, and coronal) and three different wavelengths: 405, 532, and 635 nm. A large database of the brain optical properties is produced by slicing the tissue and measuring these parameters in each slice followed by mapping the measurements to the atlas of rat brain.³² The 3-D simulation software is able to incorporate the effect of tissue heterogeneities, physical parameters of the source (e.g., optical fiber core diameter, NA, or beam type, such as uniform or Gaussian), and offers

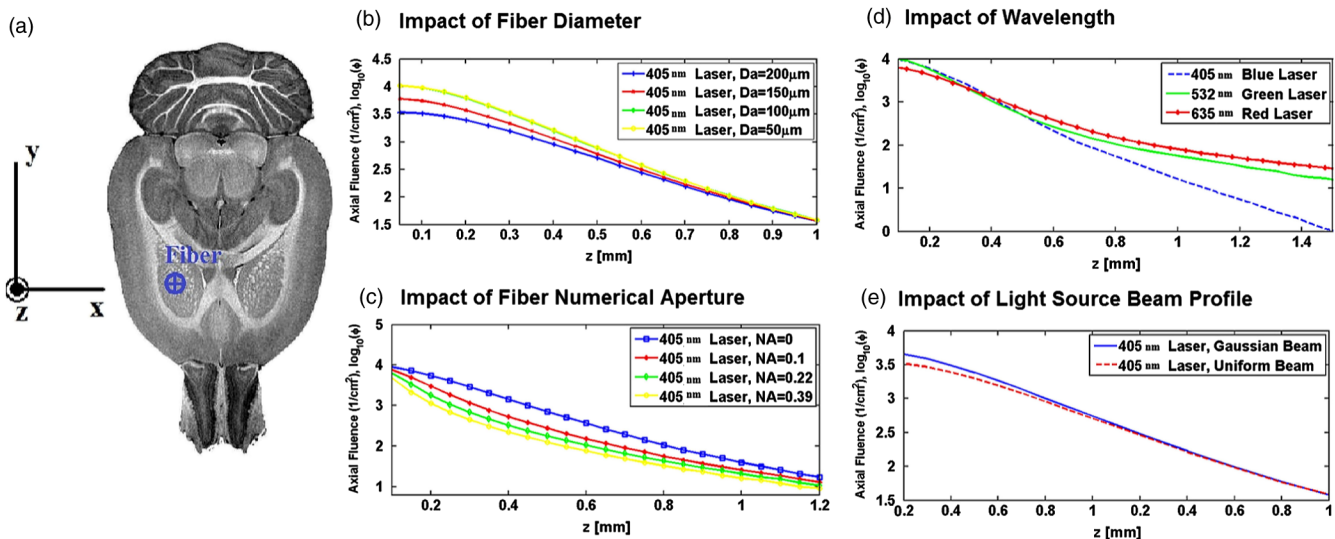


Fig. 9 (a) An optical fiber is placed on the marked area and the Monte Carlo simulation software is used to investigate the effect of source parameters on light distribution inside the brain tissue for a blue laser at 405 nm. (b) Effect of the fiber diameter. (c) Effect of fiber numerical aperture. (d) Spectral response. (e) Effect of the beam profile on the axial distribution of light.

a more accurate model for prediction of light distribution in the brain. When designing an experiment to optogenetically stimulate an area inside the brain, some decisions should be made regarding the physical parameters of the fiber and the intensity of light required to generate effective stimulation in the tissue. The integration of the rat brain atlas and the 3-D Monte Carlo software can provide a useful toolbox and the simulations can help to choose these parameters more accurately, which certainly improves the quality of the results and the rate of success, particularly for *in vivo* optogenetic experiment. One aspect in tissue light interaction that is not discussed in the current manuscript is the effect of blood on light distribution and penetration. Previous experiments have shown that mammalian blood has relatively high absorption and scattering coefficients,³³ and incorporating the optical properties of the blood in the models potentially improves the precision of the predictions. One possible approach to include the effect of blood is to use advanced optical imaging methods, such as optical coherence tomography, to scan the tissue and generate angiograms, which provide insight to the details of blood distribution in the tissue under test. Next, this angiogram can be integrated into the developed brain atlas of optical properties, which is used for Monte Carlo simulations.

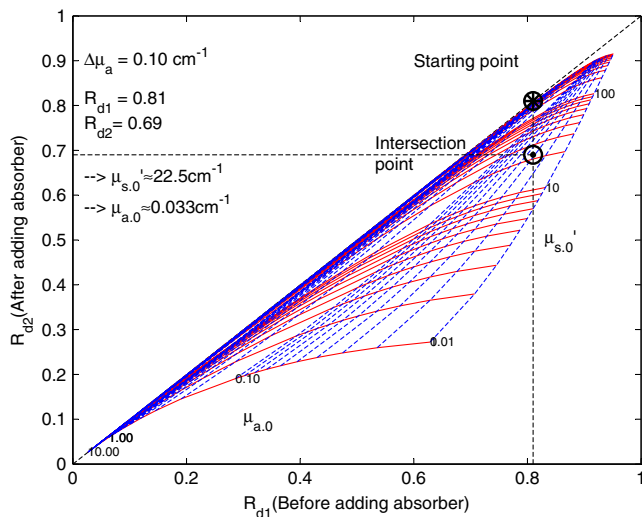


Fig. 10 Optical properties of a phantom can be determined by measuring total diffuse reflectance before and after adding an absorber with known absorption coefficient. This grid represents the contours of constant absorption and reduced scattering coefficient for the added absorber of $\mu_a = 0.1 \text{ cm}^{-1}$.

Although brain tissue and optogenetic neurostimulation was the main target in this study, the proposed approach for extracting optical properties and predicting the light distribution can be adapted as a general method for other tissue samples and different applications, such as laser surgery, laser therapy, optical tomography, etc.

Appendix A: Evaluating the Performance of the Scanning System by Using Calibrated Phantom

To evaluate the performance of the proposed approach in extracting optical properties, including the process of making the measurements using the scanning system that is shown in Fig. 2 and the application of the inverse adding doubling algorithm to reconstruct the optical properties, a calibrated phantom with known optical properties was needed. For this purpose, 1% milk was used as a calibrated phantom for which the optical properties were measured by using the added absorber method.³⁴ The added absorber method clarifies the reduced scattering and absorption coefficients of a homogenous semi-infinite medium by measuring its diffuse reflectance before and after adding some absorbing material (such as India ink solution) with a known absorption coefficient to the medium. Then these measurements are used to solve a system of equations to obtain the reduced scattering and absorption coefficients. In the added absorber method, we assume that adding an absorber does not change the scattering coefficient.

In our experiment, we measured the diffuse reflectance of 1% milk (R_{d1}). Then, some India ink was added to the sample to increase its absorption coefficient by 0.1 cm^{-1} and the same parameter was measured again (R_{d2}). By having these two measurements, the absorption and reduced scattering coefficients of the original phantom were determined using the grid shown in Fig. 10. This grid represents the contours of constant absorption and reduced scattering coefficients for the added absorber of $\mu_a = 0.1 \text{ cm}^{-1}$. The first point (marked by \otimes) shows the total diffuse reflectance before and the second point (marked by \odot) shows the total diffuse reflectance after adding the absorber, and the intersection determines the properties of the original phantom, which, in our case, was $\mu_a = 0.033 \text{ cm}^{-1}$ and $\mu'_s = 22.5 \text{ cm}^{-1}$. To validate the accuracy of our system in extracting the optical properties, agaros gel and the calibrated phantom (1% milk) were mixed to prepare a solid phantom with a thickness of $500 \mu\text{m}$. By using our technique, the optical properties were estimated to be $\mu_a = 0.025 \text{ cm}^{-1}$ and $\mu'_s = 20.49 \text{ cm}^{-1}$. Compared to the calibrated phantom

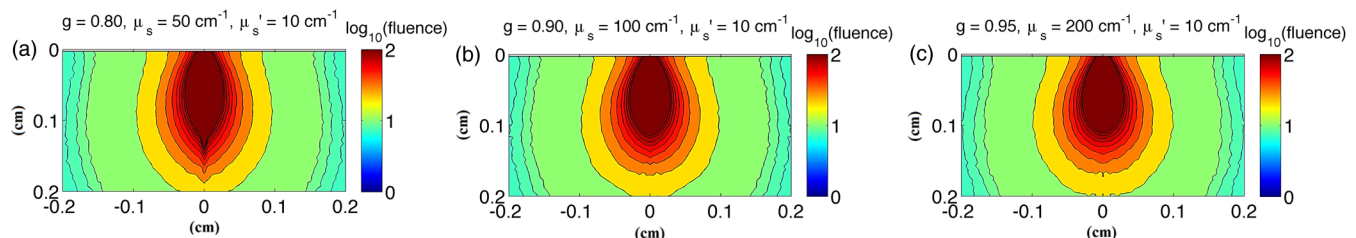


Fig. 11 The similarity principle is pertinent within the region of nondiffuse light propagation near the light source. Holding μ'_s constant at 10 cm^{-1} , the relative fluence rate ($1/\text{cm}^2$) is similar despite changes in g and μ_s . (a) $g = 0.80$, $\mu_s = 50 \text{ cm}^{-1}$, $\mu'_s = 10 \text{ cm}^{-1}$. (b) $g = 0.90$, $\mu_s = 100 \text{ cm}^{-1}$, $\mu'_s = 10 \text{ cm}^{-1}$. (c) $g = 0.95$, $\mu_s = 200 \text{ cm}^{-1}$, $\mu'_s = 10 \text{ cm}^{-1}$. Figure shows isofluence-rate contour lines.

properties, the reconstructed values show 21% error for the absorption coefficient and 9% for reduced scattering coefficient.

Appendix B: Similarity Principle

The similarity principle says that light distributions are specified by the lumped parameter $\mu'_s = \mu_s(1 - g)$. While widely understood for diffuse light propagation, it is not widely appreciated that this principle also pertains to the nondiffuse regime near the entry point of light into tissue where diffusion theory is not accurate. Figure 11 shows the pattern of fluence rate near the position where light is launched into a tissue. The reduced scattering coefficient, μ'_s , is kept constant at 10 cm^{-1} , while the value of g is varied from 0.8 to 0.9 to 0.95, and $\mu_s = \mu'_s/(1 - g)$. The light distributions are basically the same for all cases. As the g value drops below 0.5, there is an on-axis penetration of light that develops. Figure 11 for $g = 0.8$ shows the early formation of this on-axis penetration. For tissues, which typically present $g \geq 0.8$, the similarity principle means predictions of light distribution depend on μ'_s and are not strongly dependent on the accuracy of μ_s and g .

Acknowledgments

This research was sponsored by the University of Wisconsin Intercampus award under grant number UDDS B19-2510. Data for multidimensional magnetic resonance histology atlas of the Wistar rat brain are supplied by the Duke Center for In Vivo Microscopy.

References

1. E. S. Boyden et al., "Millisecond-timescale, genetically targeted optical control of neural activity," *Nat. Neurosci.* **8**, 1263–1268 (2005).
2. F. Zhang et al., "Circuit-breakers: optical technologies for probing neural signals and systems," *Nat. Rev. Neurosci.* **8**, 577–581 (2007).
3. F. Zhang et al., "Multimodal fast optical interrogation of neural circuitry," *Nature* **446**, 633–639 (2007).
4. F. Zhang et al., "Optogenetic interrogation of neural circuits: technology for probing mammalian brain structures," *Nat. Protoc.* **5**(3), 439–456 (2010).
5. K. Deisseroth, "Optogenetics," *Nat. Methods* **8**(1), 26–29 (2010).
6. L. Fenno, O. Yizhar, and K. Deisseroth, "The development and application of optogenetics," *Annu. Rev. Neurosci.* **34**, 389–412 (2011).
7. O. Yizhar et al., "Optogenetics in neural systems," *Neuron* **71**(1), 9–34 (2011).
8. R. Pashaie et al., "Optogenetic brain interfaces," *IEEE J. Rev. Biomed. Eng.* **7**, 3–30 (2014).
9. J. Mattis et al., "Principles for applying optogenetic tools derived from direct comparative analysis of microbial opsins," *Nat. Methods* **9**(2), 159–172 (2011).
10. D. Dudley, W. Duncan, and J. Slaughter, "Emerging digital micromirror device (DMD) applications," *Proc. SPIE* **4985**, 14–25 (2003).
11. R. Prakash et al., "Two-photon optogenetic toolbox for fast inhibition, excitation and bistable modulation," *Nat. Methods* **9**, 1171–1179 (2012).
12. V. Nikolenko et al., "SLM microscopy: scanless two-photon imaging and photostimulation with spatial light modulators," *Front Neural Circuits* **2**, 1–14 (2008).
13. R. Pashaie and R. Falk, "Single optical fiber probe for fluorescence detection and optogenetic stimulation," *IEEE Trans. Biomed. Eng.* **60**(2), 268–280 (2013).
14. R. Pashaie and R. Falk, "Spectral analysis of whisking output via optogenetic modulation of vibrissa cortex in rat," *Biomed. Opt. Express* **4**(1), 122–133 (2013).
15. A. Aravanis et al., "An optical neural interface: in vivo control of rodent motor cortex with integrated fiberoptic and optogenetic technology," *J. Neural Eng.* **4**(3), S143–156 (2007).
16. T. Vo-Dinh, *Biomedical Photonics Handbook*, 1st ed., CRC Press, Boca Raton, Florida (2003).
17. E. Stark, T. Koos, and G. Buzsaki, "Diode probes for spatiotemporal optical control of multiple neurons in freely moving animals," *J. Neurophysiol.* **108**, 349–363 (2012).
18. S. I. Al-Juboori et al., "Light scattering properties vary across different regions of the adult mouse brain," *PLoS ONE* **8**(7), e67626 (2013).
19. S. L. Jacques, "Optical properties of biological tissues: a review," *Phys. Med. Biol.* **58**(11), R37–R61 (2013).
20. S. L. Jacques et al., "Measuring tissue optical properties in vivo using reflectance-mode confocal microscopy and OCT," *Proc. SPIE* **6864**, 68640B (2008).
21. M. S. Patterson, B. Chance, and B. C. Wilson, "Time resolved reflectance and transmittance for the noninvasive measurement of tissue optical properties," *Appl. Opt.* **28**, 2331–2336 (1989).
22. M. S. Patterson et al., "Frequency-domain reflectance for determination of the scattering and absorption properties of tissue," *Appl. Opt.* **30**, 4474–4476 (1991).
23. T. J. Farrell, M. S. Patterson, and B. C. Wilson, "A diffusion theory model of spatially resolved, steady-state diffuse reflectance for the non-invasive determination of tissue optical properties in vivo," *Med. Phys.* **19**, 879–888 (1992).
24. J. W. Pickering et al., "A double integrating sphere system to measure the optical properties of tissue," *Appl. Opt.* **32**, 399–410 (1993).
25. S. A. Prahl, M. J. C. van Gemert, and A. J. Welch, "Determining the optical properties of turbid media by using the adding-doubling method," *Appl. Opt.* **32**, 559–568 (1993).
26. S. L. Jacques et al., "3D Monte Carlo simulation of heterogeneous tissues," <http://omlc.ogi.edu/software/mc/mcxyz/index.html> (September 2013).
27. L. Wang, S. L. Jacques, and L. Zheng, "MCML-Monte Carlo modeling of light transport in multi-layered tissues," *Comput. Methods Programs Biomed.* **47**, 131–146 (1995).
28. H. Tejada, T. Li, and S. Mohanty, "Comparison between Bessel and Gaussian beam propagation for in-depth optogenetic stimulation," *Proc. SPIE* **8586**, 85860G (2013).
29. "What is Telecentricity?," Edmund Optics Inc., <http://www.edmundoptics.com/technical-resources-center/imaging/telecentricity-and-telecentric-lenses-in-machine-vision/> (December 2013).
30. A. Ishimaru, *Wave Propagation and Scattering in Random Media*, Academic, New York (1978).
31. R. G. Keys, "Cubic convolution interpolation for digital image processing," *IEEE Trans. Acoust., Speech, Signal Process.* **29**(6), 1153–1160 (1981).
32. G. A. Johnson et al., "A multidimensional magnetic resonance histology atlas of the Wistar rat brain," *Neuroimage* **62**(3), 1848–1856 (2012).
33. N. Bosschaert et al., "A literature review and novel theoretical approach on the optical properties of whole blood," *Lasers Med. Sci.* **29**(2), 453–479 (2014).
34. B. C. Wilson, "Measurement of tissue optical properties: methods and theories," Chapter 8 in *Optical-Thermal Response of Laser Irradiated Tissue*, A. J. Welch and M. J. C. van Gemert, Eds., pp. 233–274, Plenum, New York (1995).

Mehdi Azimipour completed his Bachelor of Science in biomedical engineering from Amirkabir University of Technology and his master's degree from Shahid Beheshti University, both in Tehran, Iran, in 2005 and 2008, respectively. He is now seeking his PhD degree in the Electrical Engineering Department at the University of Wisconsin-Milwaukee. His main line of research is currently concentrated on optical imaging, optogenetic neurostimulation, and the development of advanced *in vivo* fluorescent tomography instrumentation.

Ryan Baumgartner received a BS degree in electrical engineering from the University of Wisconsin-Milwaukee, where he is currently continuing his education as a graduate student, and he is a member of the Bio-Inspired Sciences and Technologies Laboratory (BIST-Lab).

Yuming Liu is a visiting scientist at the Laboratory for Optical and Computational Instrumentation, University of Wisconsin-Madison.

He received his PhD degree in control science and engineering at Zhejiang University in China. He has authored about 20 papers in peer-reviewed journals. His research interests include Monte Carlo modeling of light transport in biological tissues, optical coherence tomography, multiphoton and second harmonic generation microscopy, and biomedical image processing with emphasis on analyzing tumor-associated collagen signatures.

Steven L. Jacques received a BS degree in biology from M.I.T., an MS degree in electrical engineering and computer science, and a PhD degree in biophysics and medical physics from the University of California-Berkeley (1984). In 1996, he joined the Oregon Health and Science University in Portland, where he now serves as a professor of dermatology and biomedical engineering. His work continues on developing novel uses of optical technologies for both therapy and diagnosis.

Kevin Eliceiri is a known expert in advanced light microscopy in the Laboratory for Optical and Computational Instrumentation (LOCI) at University of Wisconsin–Madison. The mission of LOCI is to develop advanced optical and computational techniques for imaging and experimentally manipulating living specimens. He has initiated research collaborations with faculty across the university. He is also the principal investigator of a National Institutes of Health–funded project to develop software to annotate and archive microscopy data.

Ramin Pashaie is an assistant professor in the Electrical Engineering Department at the University of Wisconsin-Milwaukee and director of the BIST-Lab. His current research is focused on the study of brain dynamics using the tools of optics, electronics, and molecular genetics. In particular, he is currently interested in implementation of neuro-prosthetic devices to extract details of information processing in cortical networks of the mammalian brain.